Accelerated Assessment of ASR Damage by Nonlinear Ultrasonic Method

Principal Investigator: Professor Jianmin Qu

A final report submitted to the Infrastructure Technology Institute

1 Accelerated Assessment of ASR Damage by Nonlinear Ultrasonic Method

1.1 Research Background

Alkali-silica reaction (ASR) is a deleterious chemical process that may occur in cement-based materials such as mortars and concretes, where the hydroxyl ions in the alkaline solution attack the siloxane groups (Si-O-Si) of the siliceous mineral components in the aggregates. Aggregates containing siliceous minerals are known to be particularly susceptible to this reaction[1-3]. Hydroxyl ions together with alkali metal cations (sodium or potassium) bind with siliceous species derived from the reactive minerals to form a cross-linked alkali-silica gel, see Fig. 1.1. The alkali-silica gel swells in the presence of water from the surrounding material[4, 5]. Expansion of the gel results in cracking when the swelling stress exceeds the tensile strength of the paste or aggregates, see Fig. 1.1. As expansion increases, cracks grow and eventually coalesce; the strength and modulus of the material are decreased and the permeability is increased. The cracking produced by ASR can significantly undermine the durability of concrete structures and may result in reduced service life.

Although the precise mechanisms of ASR formation are not completely understood yet, it is well-accepted that there are four stages in ASR damage development: (1) gel formation, (2) internal pressure buildup, (3) microcrack initiation, and (4) crack growth.
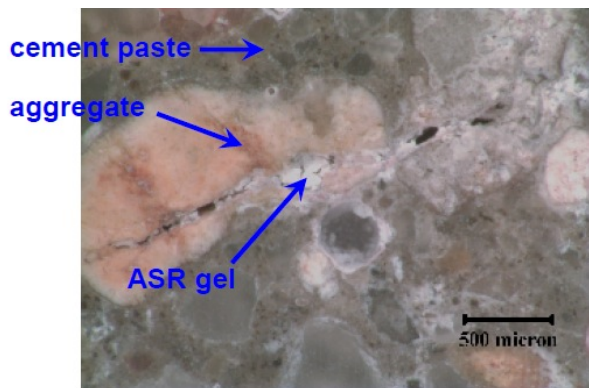
Fig. 1.1. Cross-linked alkali-silica gel from ASR.

Figure 1.2. ASR damage in concrete structures.

Severe consequences of the ASR damage include reduced strength and increased permeability. It is thus crucial to reduce the alkali loading in concrete (e.g., use low alkali cement, reduce cement content, or limit use of alkali-containing deicers) and utilize aggregates with low alkali-reactivity to minimize the occurrence of ASR where exposure to moisture in service is anticipated. However, routine testing to determine alkali-reactivity of aggregates can be challenging, because the demand of aggregates in the concrete industry is exceedingly large, and the reactivity of aggregates is a variable, even within a single source. In addition, with increasing concrete alkali contents (stemming from both increasing cement alkali contents and increasing cement contents in concrete over recent decades), growing use of higher alkali supplementary cementitious materials (SCMs), and external deicing agents, screening of aggregates for

alkali-reactivity is more critical than ever. Therefore, it is of great interest for the industry to establish a standard testing method to determine the alkali-reactivity of aggregates rapidly and reliably.

Currently, petrographic analysis and expansion tests are the most commonly used methods for characterizing the alkali-reactivity of aggregates. Petrographic examinations are commonly used to evaluate the mineral compositions of aggregates, including identification and quantification of ASR reactive minerals. By approximating the volume fraction of reactive minerals, an aggregate may be determined to be potentially reactive. However, petrographic analysis cannot be used to designate an aggregate as non-reactive because some reactive phases may not be indentified by optical microscopy. Moreover, petrography examination of aggregates are generally time consuming to perform and may require additional testing to validate the initial analysis.

Expansion test methods assess ASR damage based on length change of the mortar or concrete specimens when exposed to accelerated ASR conditioning. Despite their simplicity and low-cost nature of these expansion test methods, the long testing duration (1-2 years for ASTM C1293) makes many of them unrealistic for routine testing in practice. Accelerated mortar bar tests, such as ATSM C1260 and ASTM C1567, can be completed in a relatively short period (14 days of exposure) but they are commonly performed every three years or less and considered overly severe due to their extreme test environment including the high temperature and high alkaline storing solution for samples. This prevents the field application of these methods to existing concrete structures.

Inherent to the expansion methods is that they all rely on measuring the length change. Such change occurs primarily during microcrack initiation and crack growth, i.e., the later stages of ASR damage development. Therefore, these methods are not effective in detecting early ASR damage. Another crucial shortcoming of the expansion tests is that length measurement is a bulk assessment of ASR damage. They are unable to characterize the spatial variation of the ASR damage.

1.2 General Methodology

One-dimensional longitudinal wave motion in a nonlinear solid is governed by the equation below

$$\frac{1}{c^2}\frac{\partial^2 u}{\partial t^2} - \frac{\partial^2 u}{\partial x^2} = \frac{\partial}{\partial x}\left(\frac{\beta}{2}\left(\frac{\partial u}{\partial x}\right)^2 \right), \tag{1.1}$$

where c is the longitudinal wave velocity, u is the displacement, and β is the acoustic nonlinearity parameter. The premise here is that β is related to the ASR damage in concrete. Our goal is thus to measure β using ultrasonic techniques.

To this end, one can generate an ultrasonic wave with two frequencies ω_1 and ω_2,

$$u_1 = U\cos\left[\omega_1\left(t - \frac{x}{c}\right)\right] + V\cos\left[\omega_2\left(t - \frac{x}{c}\right)\right], \tag{1.2}$$

where U and V are, respectively, the displacement amplitude of these two frequency components.

As the wave propagates through the test sample, ASR damage in the sample causes these two frequency components to interact, resulting in a mixed wave field whose amplitude is proportional to β,

$$u_2 = -\frac{UV\beta\omega_1\omega_2}{4c^2}x\cos\left[\left(\omega_1-\omega_2\right)\left(t-\frac{x}{c}\right)\right]+\frac{UV\beta\omega_1\omega_2}{4c^2}x\cos\left[\left(\omega_1+\omega_2\right)\left(t-\frac{x}{c}\right)\right]$$

$$+\frac{U^2\beta\omega_1^2}{8c^2}x\cos\left[\left(2\omega_1\right)\left(t-\frac{x}{c}\right)\right]+\frac{V^2\beta\omega_2^2}{8c^2}x\cos\left[\left(2\omega_2\right)\left(t-\frac{x}{c}\right)\right]$$

$$\text{.} \quad (1.3)$$

In this work, we will focus on the first term in the high-hand side of Eq.(1.3), i.e.,

$$u_{2d} = -\frac{UV\beta\omega_1\omega_2}{4c^2}x\cos\left[\left(\omega_1-\omega_2\right)\left(t-\frac{x}{c}\right)\right] \quad \text{.} \tag{1.4}$$

By measuring the amplitude $\|u_{2d}\|$, one can obtain the acoustic nonlinearity parameter

$$\beta \propto \frac{\|u_{2d}\|}{UV}. \tag{1.5}$$

This way of measuring the acoustic nonlinear parameter β is called the nonlinear wave mixing (NWM) method.

1.3 Samples Preparation and Experiment Setup

1.3.1 Samples Preparation

Concrete bar samples were prepared using a procedure described by AASHTO T 303[6]. The fine aggregates used are the Placitas 67 Blend from Lafarge Company. The cement used is the type I cement (potential Bogue composition 46.11% C_3S, 22.93% C_2S, 8.52% C_3A and 9.59% C_4AF and 0.83% Na_2O_{eq}).

So far, we have made three thicker 285×100×100mm ($11^1/_4$×4×4in), and 6 thinner $285\times25\times25$mm ($11^1/_4$×1×1in) concrete bars. These samples are named, respectively, L1, L2 and L3 for the thicker ones, and S1 – S6 for the thinner ones. To cure the samples, molds with the concrete mix in them were placed in a chamber with 100% relative humidity at 23 ℃ (73.4 ℉) for 24 hours. After demolding, the samples were immersed in tap water and placed in an oven at 80 ℃ (176 ℉) for another 24 hours. The first set of expansion and nonlinear ultrasonic measurement were then taken on these as cured samples to obtain the initial values. These values were used as the baseline to normalize the subsequent measurements.

To induce ASR damage, the thinner samples S1, S2 and S3 and the thicker samples L1 and L3 were immersed in a 1N NaOH solution at 80℃ (176 ℉), per the procedures described in AASTHO T 303[6]. These samples were taken out of the solution at regular intervals for expansion and nonlinear ultrasonic measurements. The rest of the samples were left in an ambient room environment with approximately 50%RH and 23^0C.
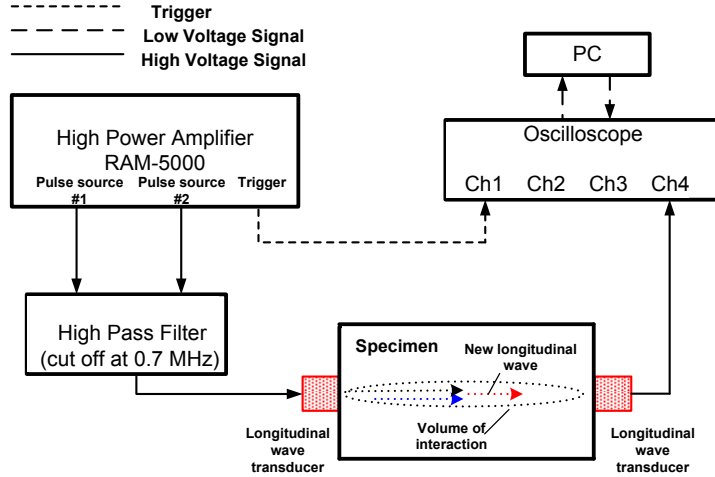
Fig. 1.3. Experiment setup for using the NWM method

1.3.2 Measuring the Ultrasonic Nonlinearity Parameter β using the NWM Method

To use the NWM method described above for measuring ASR damage, two PZT transducers are needed, one is attached to a lateral side of the concrete bar with a rectangular cross section, and the other to the opposite side of the bar, see Fig. 1.3.

In the test, two sinusoidal signals of frequencies ω_1 and ω_2 are generated by a function generator. After amplification, these signals are sent to the PZT transducer attached to one side of the sample. The PZT transducer converts the electrical signal into a propagating ultrasonic wave field in the concrete bar. This wave field consists of two frequency components as shown in Eq.(1.2). As the wave propagates, it interacts with the ASR damage in the sample. This interaction generates the mixed wave fields that consists several different frequency components. One of these frequency components is $(\omega_1 - \omega_2)$. The amplitude of this frequency component $\|u_{2d}\|$ can be obtained by performing a Fourier transform of the received signal. Once $\|u_{2d}\|$ is measured, the ultrasonic nonlinear parameter β can be calculated from Eq.(1.5), since U and V are known input.

1.4 Results and Discussion

1.4.1 Expansion Measurements and Results

The immersed samples were taken out each day for the expansion measurements per the procedures described in AASHTO T 303[6]. Results of the expansion per unit length for all samples are plotted in Fig. 1.4 as functions of the number of days under alkali solution exposure.
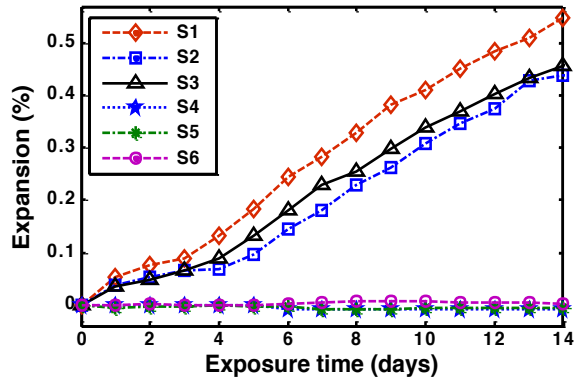
Fig. 1.4a. Expansion of the thinner samples. S1, S2 and S3 were immersed in the alkali solution, and S4, S5 and S6 were kept in a room environment.
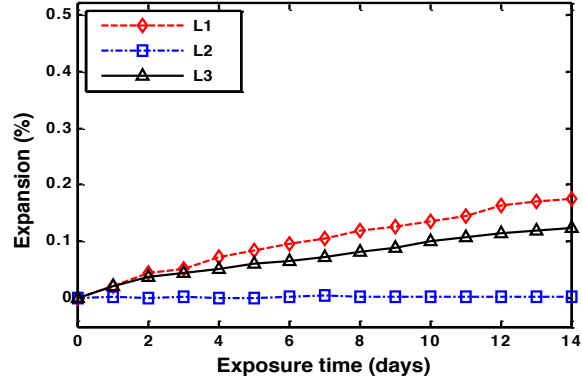
Fig. 1.4b. Expansion of the thicker samples. L1 and L3 were immersed in the alkali solution, and L2 was kept in a room environment.

It is seen that samples immersed in the alkali solution all expanded. According to ASTM1260, if the expansion of thinner samples is more than 0.2% after 14 days immersed in alkali solution, it is considered deleterious expansion. Based on this criterion, our expansion measurement data show that the aggregate used in our test, the Placitas 67 Blend from the Lafarge Co. in New Mexico, is considered fairly alkali–silica reactive. It is also seen that the samples kept in the room environment did not expand at all. If any, there seems to be some shrinkage, possibly due to the experimental errors.

Comparison between Figs. 1.4a and 1.4b shows that the thinner samples have much large expansion than the thicker samples under the same exposure time. A plausible explanation of this difference is that the ASR damage across the bar's thickness is nonuniform. The damage is more sever near the sample surface and gradually decreases toward the center of the samples. Such non-uniformity is controlled by the rate of diffusion of water into the concrete. The diffusion rate-controlled process means that the center region of the thicker samples may not have been damaged yet under 14 days of exposure. In other words, after 14 days of exposure, the thicker samples may still contain a core of un-damaged concrete, which limits the axial expansion of the bar.

1.4.2 Ultrasonic Measurements and Results

After the expansion measurement, ultrasonic tests were also conducted on each sample using the NWM method. As indicated in Fig. 1.5, the ultrasonic tests were conducted at three locations on each sample and the results reported are the average measurements from these three locations.

5
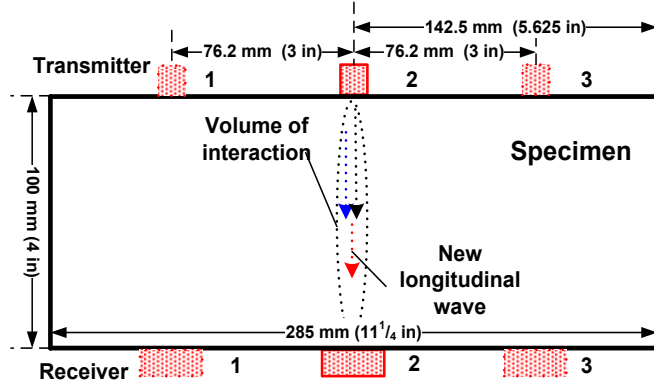
Fig. 1.5. Locations of nonlinear ultrasonic measurement on each sample
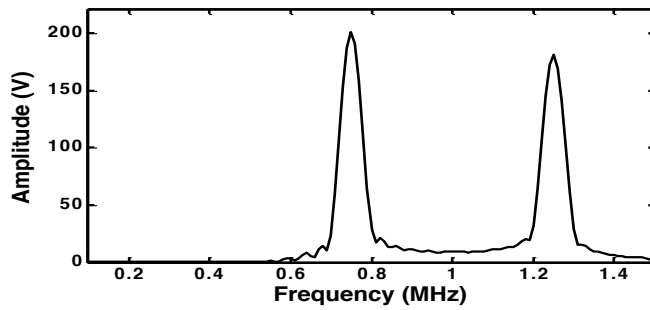
Fig. 1.6. Frequency spectrum of electrical signal after passing the high pass filter

The two frequency components in the incident wave were generated by a 0.5 in diameter broadband transmitter with a central frequency of 1.0MHz. The mixed waves are received by a 1.0 in diameter broadband receiver with a central frequency of 0.5MHz. A high-vacuum grease was used as a couplant between the transducer and the sample. A force sensor is used to ensure that the transducers were clamped to the sample with the same pressure for all tests. After each measurement, the sample was cleaned with soap and tap water to remove any residual couplant.

The experiment setup for the ultrasonic measurement is shown in Fig. 1.3. The two frequencies used are $\omega_1 = 1.25\text{MHz}$ and $\omega_2 = 0.75\text{MHz}$, so that the frequency of our interest is $\omega_1 - \omega_2 = 0.5\text{MHz}$. To match the pulse duration, 30 cycles of 1.25MHz and 18 cycles of 0.75MHz were generated. To avoid any nonlinear effect of the amplifier, a high pass filter with cut-off frequency of 0.7MHz was used between the amplifier and the transmitter to remove signals below 0.7MHz. This ensures that no frequency near 0.5MHz is transmitted into the sample by the transmitter. The frequency spectrum of the electrical signal sent to the transmitter is given in Fig. 4.6. Clearly, the signal has negligible frequency component below 0.6MHz.

As discussed before, mixing of these two frequency components in the incident wave gives rise to a new resonance wave at the difference frequency of $\omega_1 - \omega_2 = 0.5\text{MHz}$. Amplitude of this frequency component $\|u_{2d}\|$ was obtained by performing the Fourier transform of the total signal received by the receiver on the other side of the sample. It then follows from Eq.(1.5) that the normalized acoustic nonlinearity is given by

$$\bar{\beta} = \frac{\beta}{\beta_0} = \frac{\|u_{2d}\|}{\|u_{2d}\|_0}, \qquad\qquad\qquad\qquad\qquad\qquad\qquad (1.6)$$

where the quantities with subscript 0 are those measured before the samples were immersed in the alkaline solution (day 0). Subsequent ultrasonic measurements were conducted at about the same time each day during the immersion. As an example, the frequency spectra of the received signals for day 0 and day 10 are shown in Figs. 1.7a and 1.7b, respectively, for the thicker samples. It is seen that the amplitude corresponding to 0.75MHz decreases over time, a sign of increased attenuation. Such increase in attenuation is frequency dependent, and can be accounted for by measuring the decay in the fundamental waves over time. After accounting for the attenuation, the measured acoustic nonlinearity parameter $\bar{\beta}$ normalized by the day 0 value as defined in Eq. (1.6) is plotted in Fig. 4.8a for all three thicker samples. We note again that these values are the averages of measurements from all three locations on each sample. To show the scattering of the data, Fig. 4.9 are plotted with error bars. Since multiple ultrasonic measurements were conducted at each location by taking the transducers off and putting them back several times at each measurement location, these error bars are the ranges of measured values from all three locations on each sample, as well as the multiple measurements at each location.
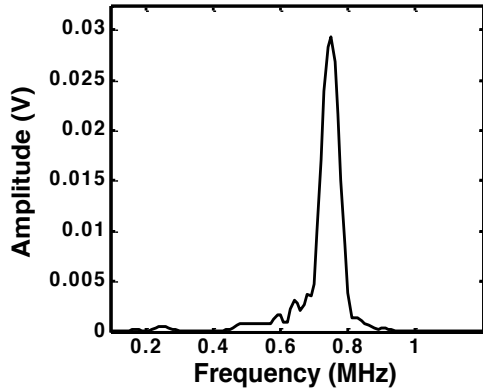
Fig. 1.7a. Frequency spectrum of the received signal on day 0.
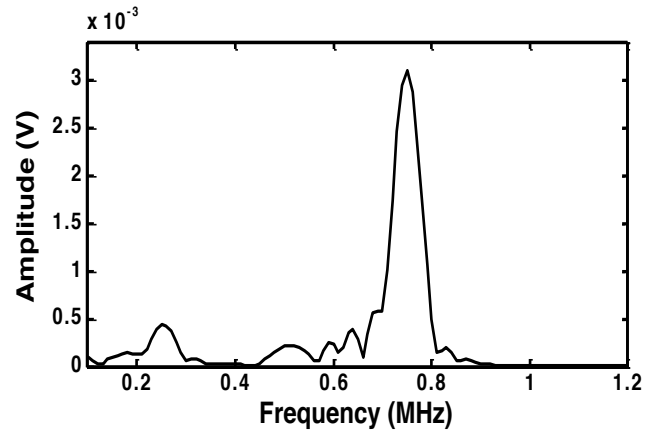
Fig. 1.7b. Frequency spectrum of the received signal on day 10.

It is seen clearly from these plots that (1) the NWM method yields consistent and repeatable results, (2) the acoustic nonlinearity parameter increases with exposure time, and (3) the acoustic nonlinearity parameter is much more sensitive to ASR damage than the volumetric expansion.

We note that results from both the ultrasonic and the expansion measurements seem to indicate that sample L1 has more ASR damage than sample L3, although both samples were made of the same materials, and were subjected to the same exposure condition. However, since these two samples were from two different batches of concrete mix, we speculate that the amount of aggregate in these two samples may not be exactly the same. We are conducting more tests to investigate this hypothesis.
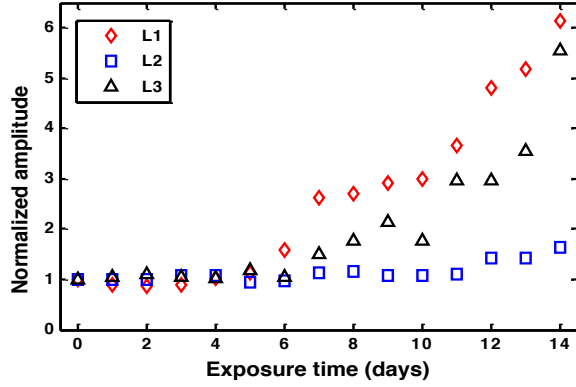
Fig. 1.8a. $\bar{\beta}$ averaged over all locations on each sample as function of exposure times.
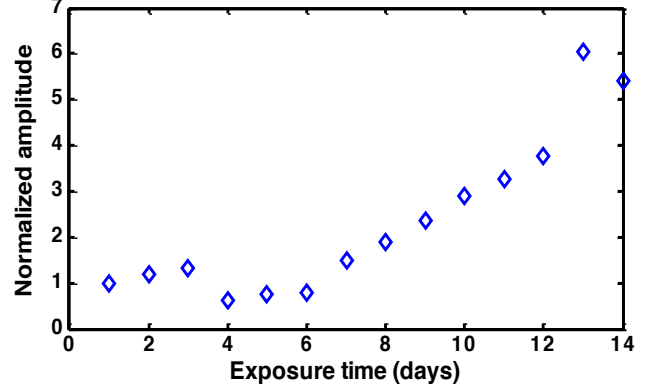
Fig. 1.8b. $\bar{\beta}$ averaged over all three locations on the thinner sample S1 as function of exposure times.

Recall that the expansion results show that the thinner samples have much larger expansion than the thicker ones. The reason for such difference was explained on the basis of non-uniform ASR damage across the thickness of the sample. It was argued that ASR damage is controlled by the moisture diffusion so that even after 14 days of exposure, the moisture still has not progressed all the way through the thickness of the thicker samples yet, i.e., there is still a core of undamaged concrete in the thicker samples. This argument is further corroborated by the ultrasonic measurement results. Shown in Fig. 1.8b is the measured acoustic nonlinearity parameter β of the thinner sample S1. Comparison of Figs. 1.8a and 1.8b shows that, although the expansion is very different between the thinner and thicker samples, the measured acoustic nonlinear parameter β is almost the same. The reason for this is clear if we assume that in the thicker sample, there is a core of concrete that has not been reached by the moisture, therefore, has no ASR damage, and the thickness of the ASR damaged outer shell is about one half of the total thickness of the thinner sample. Based on these observations, we propose the following hypothesis:

When a concrete bar is immersed in a 1N NaOH solution at 80ºC, ASR damage will be induced in an outer shell of the bar. The thickness of the ASR damaged outer shell increases with exposure time. After about 14 days, the thickness of this ASR damaged outer shell is about 12.7mm (0.5 in). Consequently, a thinner sample with cross-section of 25mm by 25mm (1.0in by 1.0in) would become fully damaged after 14 days of exposure, while the thicker sample with cross-section 100mm by 100mm (4.0in by 4.0in) will still have an undamaged core with cross-section of 75mm by 75mm (3.0in by 3.0in).
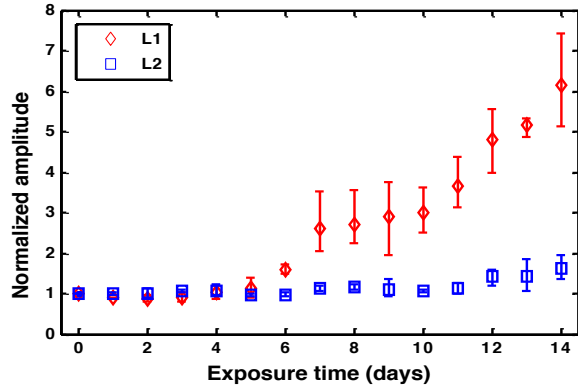
Fig. 1.9a. Error bars showing the variation of $\bar{\beta}$ for samples L1 and L2.
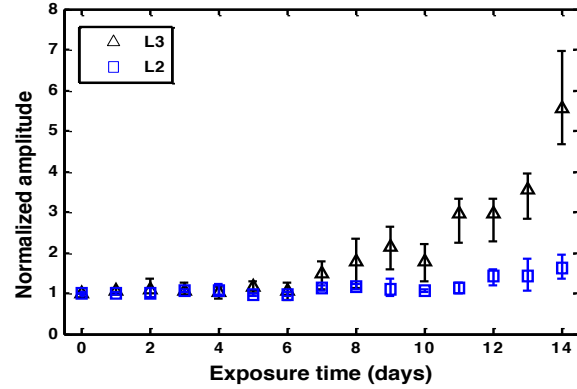
Fig. 1.9b. Error bars showing the variation of $\bar{\beta}$ for samples L3 and L2.

1.4.3 Preliminary Microscopy Results

The small sample (S1) embedded in Alkali solution was cut after the 14-days measurement to a length of 1.25cm using a low speed saw and ethanol as a lubricant. The microscopy specimens were then polished on a grinder/polisher down to 600 grit size with water, such that the surface was highly polished and the aggregates clearly visible. Digital images of the surface were taken at different locations on each specimen using a stereomicroscope at magnifications of 10X. As shown in Fig 1.10, ASR gels have filled all the boundaries between aggregates and cement pastes and the microcracks are visible too.
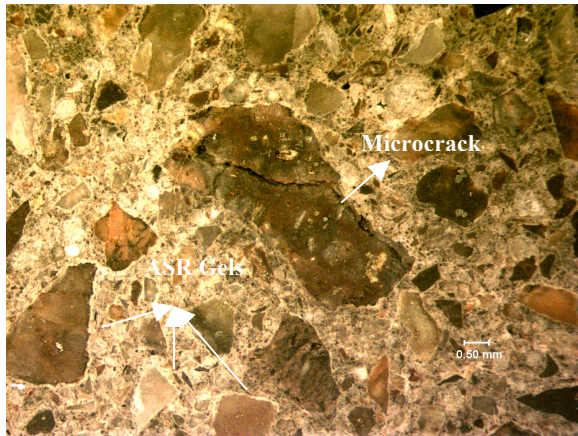
Fig. 1.10a. Microscopy in S1 after 14 days
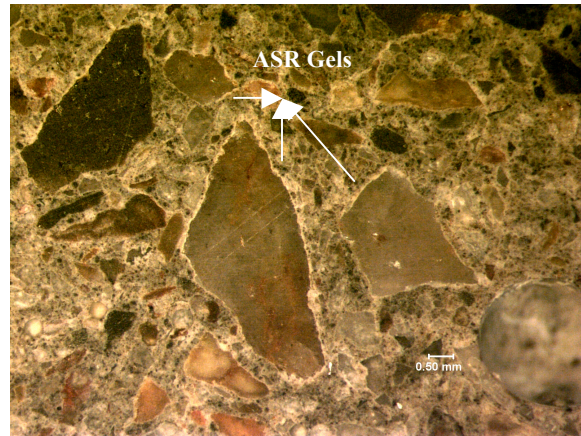
Fig. 1.10b. Microscopy in S1 after 14 days (another surface)

As a comparison, we did the similar cut on small sample (S4) which was not embedded in alkali solution and the microscopy of S4 is shown in Fig. 1.11. The boundary between aggregates and cement paste in Fig. 1.11 can be clearly discerned. Even after partial magnifying, one could easily tell there isn't any ASR on the boundary compared to Fig. 1.10b. The microscopy results are consistent with expansion and ultrasonic measurement results.
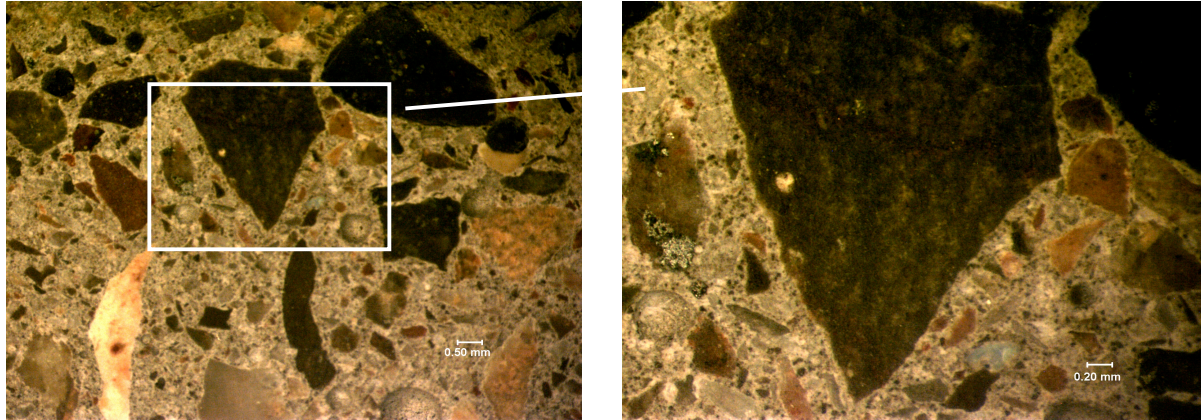
Fig. 1.11. Microscopy in S4 after 14 days

1.5 Conclusion

Among other things, our current results clearly demonstrated the feasibility of using nonlinear ultrasonic techniques to track the progress of ASR damage in concrete. This is significant in that nonlinear ultrasonic techniques have a number of unique advantages over the existing methods of characterizing ASR damage.

For example, the expansion vs. exposure time plots, see Fig. 1.4, show a linear relationship between the expansion and exposure time. However, the acoustic nonlinearity parameter shows a stepped relationship with respect to exposure time, see Fig. 1.9a, b. Although more research is needed to understand the significance of the "step", it is plausible that such a "step" might be related to the different ASR damage modes.

Comparing the expansion data to the nonlinear ultrasonic data also reveals another advantage of the nonlinear ultrasonic method. As discussed earlier, the expansion of the concrete bar depends on the thickness of the sample. This means that the expansion-based methods, such as AMBT, the CPT, and ACPT, are not measuring the intrinsic characteristics of the ASR damage and could not give us any idea of damage distribution inside mortar bar samples. On the other hand, nonlinear ultrasonic methods, such as the NWM method used here, measure the acoustic nonlinearity parameter which is a signature intrinsic to the state of ASR damage. Moreover, it enables us to measure from multiple locations of specimen and could potential make damage distribution measurement possible. Therefore, measurements from the NWM method are independent of the sample size as shown by our results.

The abilities of the nonlinear ultrasonic methods to identify the different stages of ASR damage and to track the intrinsic characteristics of the ASR damage make such methods potentially useful tools for rapid screening of aggregates for ASR reactivity in the lab, and for field assessments of ASR damage in existing concrete structures.

2 A Chemo-mechanical Model for the Acoustic Nonlinearity Change in Concrete with Alkali-silica Reactions

2.1 Introduction

Alkali-silica reaction (ASR) in concrete is a deleterious chemical reaction between the alkalis in pore solution of cement paste and the reactive silica of concrete structure aggregates. The main reaction product of this process is ASR gel [1, 2], which is located mainly in the interface zone between the aggregate and surrounding cement paste. As ASR damage progresses, more gel is produced which induces significant interface pressure, causing cracking, in concrete. The cracking produced by ASR can significantly undermine the durability of concrete structures and may result in reduced service life. It is thus necessary to develop methodologies to nondestructively assess the degree of ASR damage, and to build models to predict the structure response of damaged structures.

The most common way to evaluate ASR damage is to measure the volumetric change (expansion) of standard mortar samples. However, such change occurs primarily during microcrack initiation and crack growth, i.e., the later stages of ASR damage development. Therefore, this method is not effective in detecting early ASR damage. More importantly, this method cannot be used to actual structures in service. An alternative technique is using nonlinear ultrasonic methods to detect ASR damage. Experimental data have demonstrated that damage induced by alkali-silica reaction (ASR) in concrete, even in its very early stage, can cause changes in the acoustic nonlinearity parameter β [3, 7]. However, there is currently no model that explains the relationship between the acoustic nonlinearity parameter and ASR damage. Thus a model is needed that can quantitatively predict the nonlinearity change due to ASR damage.

2.2 Physicochemical Modeling

2.2.1 Configuration of the Microstructure

The reactive aggregate and the representative volume element (RVE) of concrete surrounding the reactive aggregate are assumed to be spherical [8]. The basic element of the microstructure in Fig. 2.1 is then a composite sphere composed of two different phases in which the ratio of radii $R_a/R_{RVE}{}^a$ is a constant. Thus the basic element is independent of the absolute size of the spheres.
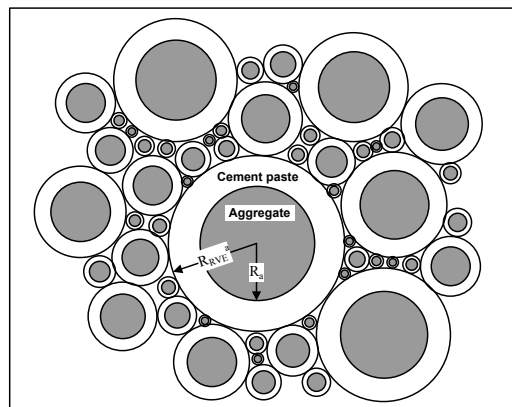
Fig. 2.1. Definition of the representative volume element for different reactive aggregate sizes

2.2.2 Mathematical Model for Diffusion of Alkali Ions

To compare with our former experiments [7], two kinds of mortar samples with the dimension of 25×25×285mm (1×1×11^1/$_4$in) and 100×100×285mm (4×4×11^1/$_4$in) respectively are considered in our numerical simulations. Alkali ions penetrating from the specimen boundary into the concrete is considered as macro-diffusion process. Symmetry of mortar bars leads to two-dimensional diffusion problem governed by the 2D Fickian Equation [9],

$$(\frac{\partial C}{\partial t})_{x,y,t} = D_{xy} \cdot (\partial^2 C / \partial x^2 + \partial^2 C / \partial y^2)$$
(2.1)

where C is the alkali ion concentration, and D_{xy} is the diffusivity of alkali ions at 80°C [10].
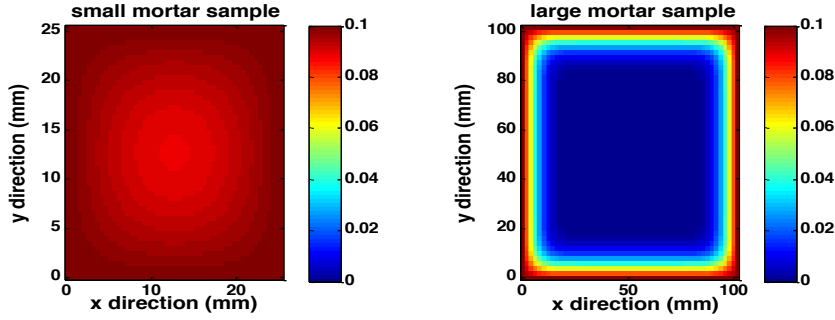
Fig. 2.2. Ion diffusion in small and large mortar samples after 14 days

Suppose the alkali ions penetrate with moisture, then D_{xy} can be determined by experimental measurements as described by Shen [9]. From Eq.(2.1), one can obtain the ion concentration, $C(x,y,t)$. As a result, after 14 days, the alkali ions has penetrated thoroughly in small mortar sample, while there is still a very large core in large mortar sample that the ion has not penetrated in as shown in Fig. 2.2. Note that the alkali ion concentration at the boundary of mortar sample is C_0=0.1 mol/liter of solution [11].

In our samples, the size of aggregates varies from 0.225mm to 3.56mm [10]. To compute the ion concentration near each aggregate, each mortar bar is divided into several layers with layer thickness of 5.34mm. As a result, there are three layers in small samples and nine layers in large samples. For simplicity, the ion concentration within each layer is assumed uniform and equal to the value at the middle point of each layer.

The micro-diffusion is the diffusion of alkali ions into the aggregate. This process can be described by Fick's law in spherical coordinate as,

$$B_{ion} \frac{\partial C_{ion}}{\partial t} = \nabla \cdot (D_{ion} \nabla C_{ion})$$
(2.2)

where C_{ion} is the free ion concentration of the pore solution inside the aggregate. B_{ion} and D_{ion} are the binding capacity and ion diffusivity of the aggregate, respectively. The initial condition is $C_{ion} = 0$ for $t = 0$ in the aggregate. The boundary condition is $C_b = C(t)$ at the surface of aggregate, and $\partial C_{ion} / \partial r = 0$ at the center of the aggregate particle. Eq.(2.2) can be solved numerically using the finite difference method.

The ASR process takes place within the surface layer of each aggregate particle, where C_{ion} reaches a certain concentration level C_{crt}. One can inversely determine the thickness of the ASR layer, r, from the numerical solution of Eq.(2.2). The volume of the reacted portion of the aggregate particle of radius R_a can then be calculated,

$$V_a^{Ra} = [\frac{R_a^3 - (R_a - r)^3}{R_a^3}](\frac{4}{3}\pi R_a^3) \tag{2.3}$$

This volume is converted into the volume of ASR gel, V_{gel}^{Ra},

$$V_{gel}^{Ra} = \eta V_a^{Ra} \tag{2.4}$$

where η is the coefficient of volumetric expansion from aggregate to ASR gel.

2.2.3 Mathematical Model for Permeation of ASR Gel into the Surrounding Cement

Because of the volumetric expansion when the aggregate is converted into ASR gel, the gel causes internal pressure near the interface zone between the aggregate and the surrounding cement. This pressure pushes the gel into the pores around this interface zone. As more pores nearby are filled up with the gel, the pressure increases, which deforms the concrete. The amount of gel that is capable of generating the internal pressure is given by

$$V_{gel,eff}^{Ra} = \langle V_{gel}^{Ra} - V_{pore}^{Ra} \rangle_+ \tag{2.5}$$

where V_{pore}^{Ra} is the total volume of pores in the surrounding interface zone that can be calculated using,

$$V_{pore}^{Ra} = V_{unit} A_{agg}^{Ra} \tag{2.6}$$

where V_{unit} is a material constant (a length scale) representing the capacity of the porous zone to absorb ASR gel per unit area, and A_{agg}^{Ra} is the surface area of an aggregate particle of size R_a. When the effective gel volume $V_{gel,eff}^{Ra}$ is larger than zero, the ASR gel begins to permeate. This process can be characterized by Darcy's law for viscous flow as,

$$\frac{\partial C_{gel}}{\partial t} = \nabla(\frac{\kappa_{gel}}{\eta_{gel}} \nabla P_{gel}) \tag{2.7}$$

in which C_{gel} and η_{gel} are the concentration and viscosity of the gel, respectively, κ_{gel} is the gel permeability of the porous cement paste, and P_{gel} is the pressure distribution of the gel, which depends on the degree of saturation of the pores. At the boundary, the interface pressure, P_{int}, is applied. However, as P_{int} is an unknown and a function of time, it needs to be calculated simultaneously from the equilibrium of the composite system (see micro-mechanical modeling), the diffusion of ions, and the permeation of the gel. So this is a coupled chemo-mechanical problem.

In order to solve the coupled equations, a state equation must be introduced, which relates the concentration of ASR gel in the pores, C_{gel}, the gel pressure P_{gel},

$$C_{gel} = \beta P_{gel} \tag{2.8}$$

where β is the state function for cement paste [11]. The initial condition is $C_{gel}(r, 0) = 0$. The boundary condition at the interface is $C_{gel}(R_a, t) = \beta P_{int}(t)$, and at the far field is $C_{gel}(R_{RVE}^a, t) = 0$. Eq.(2.7) can then be solved numerically using a finite difference method for the gel concentration as a function of radius and time, $C_{gel}(r, t)$. The gel volume in the porous cement paste can then be evaluated by integrating the gel concentration over the surrounding cement paste,

$$V_{pg}^{Ra} = \int_{R_a}^{R_{RVE}^a} 4\pi r^2 C_{gel} dr \tag{2.9}$$

The coefficient of expansion for the aggregate with radius R_a due to ASR is thus,

$$\alpha_1 = \frac{\Delta V_{gel}^{Ra}}{V_a^{Ra}} = \frac{V_{gel,eff}^{Ra} - V_{pg}^{Ra}}{V_a^{Ra}} = \frac{V_{gel}^{Ra} - V_{pore}^{Ra} - V_{pg}^{Ra}}{V_a^{Ra}} \tag{2.10}$$

2.3 Micro-mechanical Modeling

2.3.1 Three-phase Expansion Model

By a standard homogenization argument, the micro-structural configuration shown in Fig. 1 can be considered equivalent to that shown in Fig. 2.3, where phase 3 is the effective homogeneous medium equivalent to the heterogeneous medium in Fig. 2.1. Following the three-phase expansion model developed by Jin et al [12], one can obtain the effective expansion coefficient for the two-phase composite as well as the interface pressure between the aggregate and cement paste. For brevity, we only list the results here, and details can be found in [11]. The effective expansion and interface pressure can be written as,

$$\alpha_{eff} = \frac{K_a V_1 (3K_{SC} + 4G_{SC})}{K_{SC}(3K_a + 4G_{SC}) - 4V_1 G_{SC}(K_{SC} - K_a)} \alpha_1 \tag{2.11}$$

$$P_{int} = \frac{12 K_a G_{SC} K_{SC}(1 - V_1)}{4V_1 G_{SC}(K_a - K_{SC}) + K_{SC}(3K_a + 4G_{SC})} \alpha_1 \tag{2.12}$$

where K_a, K_{SC} are the bulk modulus of aggregate and cement paste matrix, respectively, G_{SC} is the shear modulus of the cement paste, and $V_1 = R_a^3 / (R_{RVE}^a)^3$ is the volume fraction of aggregate.
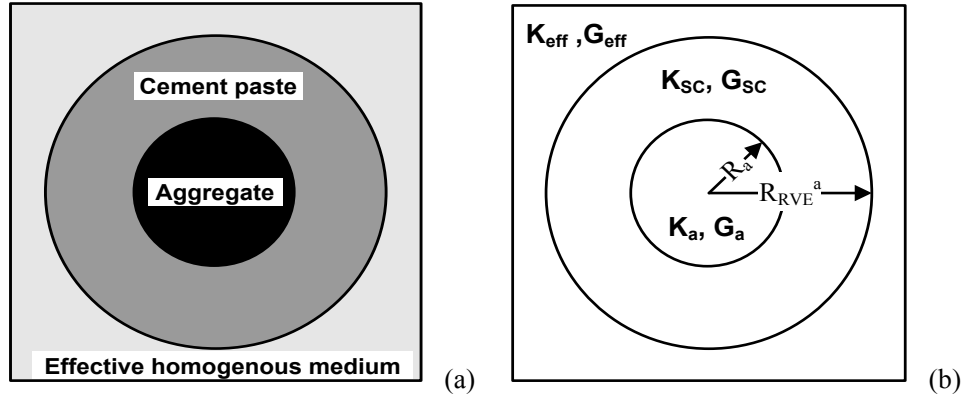
Fig. 2.3. (a) Three phase expansion model and (b) its mechanical properties

The unknown parameter in Eqs. (2.11) and (2.12) is the expansion coefficient of aggregate due to ASR, α_1, which can be evaluated by Eq.(2.10). As one can see, both α_1 and P_{int} involve the ASR gel formation due to alkali ion diffusion and the ASR gel permeation driven by interface pressure P_{int}.

2.3.2 Damaged RVE
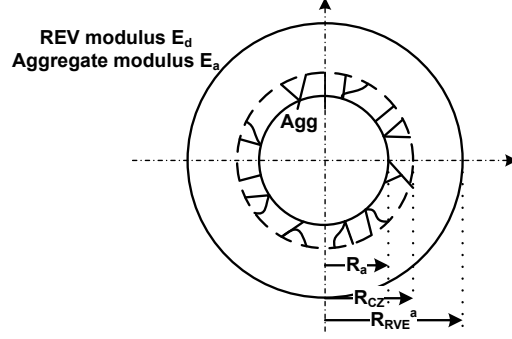
Fig. 2.4. Mechanical property of damaged RVE

Since the Young's modulus in the cement paste matrix is much lower than in the aggregate, cracks will initiate at the boundary and propagate into the cement paste matrix. According to the Griffith criterion, the critical pressure for crack initiation can be obtained,

$$P_{cr} = \sqrt{\frac{E_{SC}G_{IC}}{\pi(R_a + c_r)}} \tag{2.13}$$

where E_{SC} is the Young's modulus of cement paste, G_{IC} is the fracture energy of concrete, c_r is the initial crack length in the cement paste. Once the interface pressure P_{int} exceeds the critical pressure P_{cr}, crack starts to propagate which causes a decrease in the modulus. This can be described by a damage parameter [8], which is defined by,

$$d = \frac{R_{CZ} - R_a}{R_{RVE}^a - R_a} \tag{2.14}$$

where R_{CZ} represents the crack front as shown in Fig. 2.4. The modulus of the equivalent medium E_d can then be determined,

$$E_d = (1-d)E_{SC} \tag{2.15}$$

The newly generated cracks also increase the volume of the RVE. The amount of volume expansion induced by crack growth is given by,

$$\alpha_C = \frac{\Delta V}{V_{R_{RVE}^a}} = \frac{c_{pnew} - c_p}{1 - c_{pnew}} \cdot (1 - V_1) \tag{2.16}$$

where $V_{R_{RVE}^a} = \frac{4}{3}\pi(R_{RVE}^a)^3$ is the volume of the RVE, c_p and c_{pnew} are the porosity of cement paste matrix before and after crack opening respectively. The total expansion is the linear superposition of α_{eff} and α_C, i.e., $\alpha_{total}{}^{Ra} = \alpha_{eff}{}^{Ra} + \alpha_C{}^{Ra}$. Since the ASR induced expansion of aggregate is size dependent [11], the overall ASR expansion of concrete must be determined as the volumetric average of ASR expansion of the RVE with different sizes. For each aggregate, the final expansion should also include the volumetric average of each layer as described in macro-diffusion process. Thus the overall expansion is,

$$\alpha_{total} = \sum \phi_a \sum \phi_i^a \alpha_{total,i}^{Ra} \tag{2.17}$$

where ϕ_a is the volume fraction of aggregate with size R_a, ϕ_i^a is the volume fraction of each layer for a fixed aggregate size R_a, and $\alpha_{total,i}^{Ra}$ is the ASR expansion of the concrete located at the ith layer with the aggregate size R_a.

Equations (2.1)-(2.17) form a complete model for ASR expansion. It is unlikely to solve the problem analytically because the diffusion and the permeation of gel are coupled with the interface pressure. Instead, a piecewise numerical procedure is adopted. More details can be found in [11].

2.4 Compare Numerical Results with Experiments

Since the only unknown parameter in our numerical calculation is the crack opening speed, i.e., the increase of c_r as shown in Eq.(2.13), a set of ASR expansion measurements in small mortar samples are used to fit this model and determine this parameter. It is then used to predict the expansion of other samples. As shown in Fig. 2.5, the expansion calculated by the model based on Eq. (2.17) (red solid line) has the same trend as in experiment measurements.
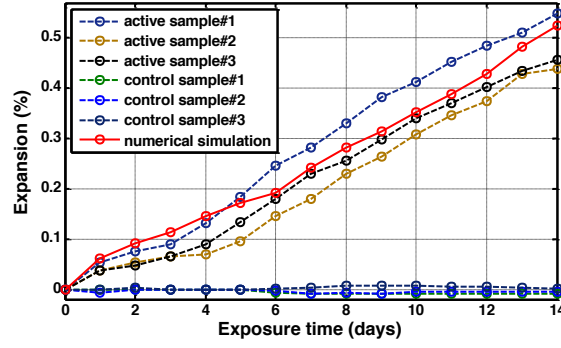
Fig. 2.5. Expansion in small mortar samples with comparison to numerical calculation

Following Cantrell's theory [13], the acoustic nonlinearity parameter in materials with dilute distribution of microcracks can be written as,

$$\beta = \beta_0 + \frac{24}{5}\frac{\Omega\Lambda_{mp}L_0^4 R^3 \overline{A_{11}^2}}{\mu^3 b^2}|\sigma_1|+(\beta' N_0^{crk}/7) \qquad (2.18)$$

where β_0 is the original material nonlinearity before cracking, σ_1 is the initial stress, N_0^{crk} is the crack density, and other parameters are all material constants. To avoid the complexity of determining these material constants, we assume that,

$$\overline{\beta} = \frac{\beta}{\beta_0}-1=\alpha|\overline{\sigma_1}|+(1-\alpha)\overline{N_0^{crk}} \qquad (2.19)$$

where $\overline{\beta}$ is the normalized acoustic nonlinearity parameter reflecting the nonlinearity change, $|\overline{\sigma_1}|$ is the initial stress (comparable to interface pressure) normalized by its maximum value, $0<|\overline{\sigma_1}|<1$, and $\overline{N_0^{crk}}$ is the crack density (comparable to damage variable d) normalized by its maximum value, $0<\overline{N_0^{crk}}<1$. For a reasonable approximation, the weight parameter α is taken in the range $0<\alpha<0.5$.

Following an equation similar to Eq.(2.17), one can obtain the volumetric averaged interface pressure and damage variable d up to 14 days exposure time as shown in Fig. 2.6(a) and (b). As one can see, in both samples, the damage becomes obvious around day 6, and afterwards, in small sample, it shows a linear increase; while in large sample, the damage

shows a faster increase after 12 days. This is because in large sample, alkali ions have only penetrated into the outer layers after 14 days as shown in Fig. 2.2. As more and more ions get into the large sample, the cracks accumulate, and as a result, the damage shows a faster increase after 12 days.
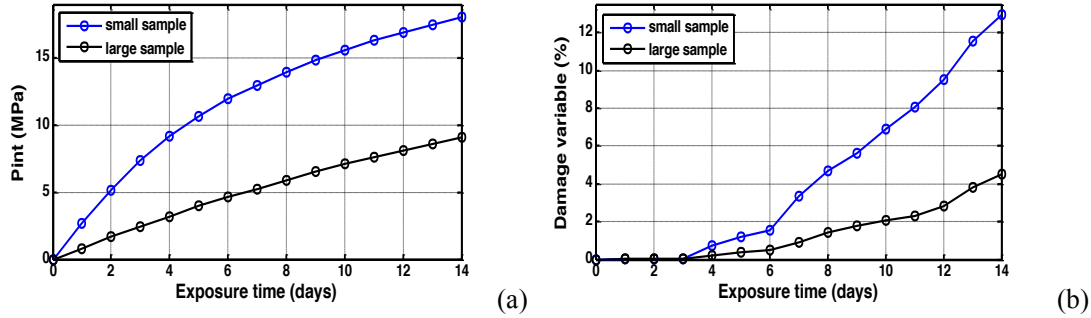
Fig. 2.6. Volumetric averaged (a) interface pressure and (b) damage variable *d* in both mortar samples
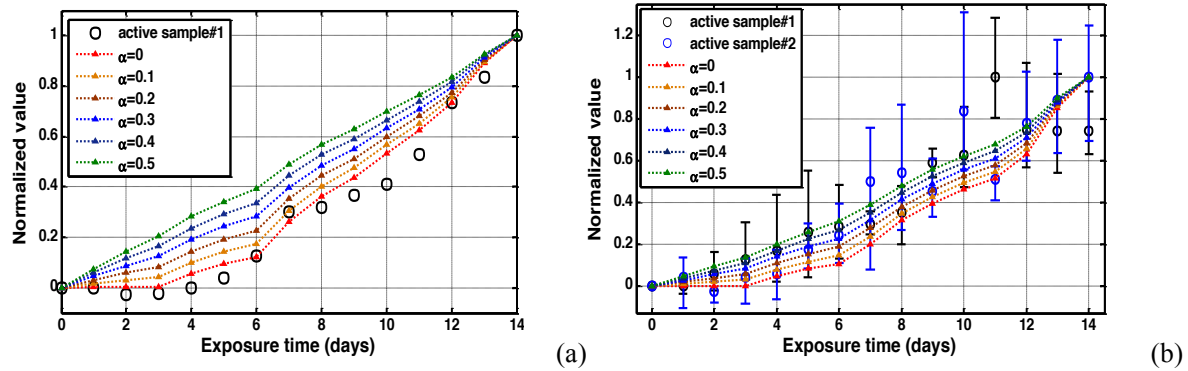
Fig. 2.7. Predicted and measured variation of $\bar{\beta}$ in (a) small and (b) large mortar samples

The predicted variation of $\bar{\beta}$ in both small and large mortar samples can be obtained from Eq. (2.19) as shown in Fig. 2.7(a) and (b) respectively. By comparing with experimental measurements, we observe in small mortar sample, when $\alpha=0$, the predicted curve compares well with experimental measurements. This is because the small sample has damage everywhere after 14 days, the nonlinearity change is microcrack dominated. While in large sample, this is not the case. As shown in Fig 2.7(b), when $\alpha=0.2$ or 0.3, the predicted curve matches better with experimental measurements. One possible explanation is that in large samples, since alkali ions have not penetrated thoroughly after 14 days, the interface pressure also contributes to the nonlinearity change. However, the results in both samples show that this numerical model can effectively predict the nonlinearity parameter jump at both day 7 and day 12. These jumps may indicate different damage stages during ASR process. Before day 6, since the ASR damage is only limited to the interface pressure built up, $\bar{\beta}$ increase is very slow. After day 6, due to the rise of crack density, $\bar{\beta}$ increase is accelerated. Finally after day 11, more cracks are formed which further reduces the Young's modulus. Consequently, there is another jump of $\bar{\beta}$. So in all, our numerical model seems to be capable of predicting the acoustic nonlinearity change.

2.5 Conclusions

This paper presents a new model to predict acoustic nonlinearity change during ASR damage. This new model includes a chemo-mechanical model, a micromechanical model and a fracture model. These models are tightly coupled. In the fracture model, a damage variable is introduced to simulate crack opening. The interface pressure and damage variable are then used to calculate the acoustic nonlinearity change. The results of numerical prediction and experimental measurements are in good agreement. Although more experiments on aggregates with different activities are needed to further validate this model, the present work has shown that the proposed method has a good potential to quantitatively predict the acoustic nonlinearity variation during ASR damage and can be used to guide experimental measurements in the future.

3   Future Work

3.1 Model Improvement

The model presented here is mainly based on a previous model developed by Jin et al.[12]. Several improvements can be noted in this new model:

- To predict the total expansion of the whole mortar sample, the consideration of macro-diffusion process has been added to assess the localized alkali ion concentration of each aggregate before conducting micro-diffusion process. By adding the macro-diffusion process, the overall expansion makes more sense since the mortar sample has certain thickness and the alkali ion concentration should not be the same for each aggregate with different locations.

- Due to the large interface pressure generated on the surface of certain aggregates, crack initiation has been added to get more accurate expansion. In this new model, damage variable is introduced. It is tightly related to the crack density, porosity, as well as Young's modulus change of cement paste matrix and finally contributes to the prediction of acoustic nonlinearity change, which is in very good agreement with experimental measurements.

However, the present model still has some limitations. First of all, the model was developed with several assumptions (about the diffusion, the composition of the ASR gel, the mechanical properties of cement paste matrix after crack initiation, etc.). Secondly, to obtain more accurate prediction of acoustic nonlinearity change, the exact micro-scale material constants as shown in Eq. (2.18) needs to be determined. Supplementary investigations are also needed before it can be applied to real structures. In particular, the effect of temperature on all the chemo-mechanical and micromechanical mechanisms needs to be analyzed.

3.2 Implementation Feasibility

The proposed measurement technique requires a basic set of ultrasonic measurement equipment, and expertise on sample preparation and ultrasonic measurement. Sample preparation is identical to the currently practiced expansion test methods such as AMBT and ACP methods. Therefore, no additional equipment and expertise are required for

sample preparation.

Ultrasonic measurement requires standard equipment such as transducers, amplifier, oscilloscope, filters, etc. These components are standard off-the-shell commercial products. Ultrasonic testing is safe and benign. No certification is required to operate ultrasonic test equipment. In fact, ultrasonic testing has been the de-facto method for non-destructive evaluation in many industries since the early 1960s.

For conducting the nonlinear ultrasonic measurement proposed here, certain expertise and proficiency are needed to interpret the data. This will be the major challenge in implementing the new technology. To overcome this challenge, effort will be made in two fronts. First, one of our Year 3 efforts will be to optimize the measurement system in order to make it more robust and more user-friendly to minimize the subjectivity of the operator. Second, we will work with the industry to transfer the technology through publications, workshops and on-site training.

4   References

1.   Chatterji, S., *Role of Ca(Oh)2 in the Breakdown of Portland-Cement Concrete Due to Alkali-Silica Reaction.* Cement and Concrete Research, 1979. **9**(2): p. 185-188.
2.   Kurtis, K.E., et al., *Imaging of ASR gel by soft X-ray microscopy.* Cement and Concrete Research, 1998. **28**(3): p. 411-421.
3.   Chen, J., et al., *Nonlinear Wave Modulation Spectroscopy Method for Ultra-Accelerated Alkali-Silica Reaction Assessment.* Aci Materials Journal, 2009. **106**(4): p. 340-348.
4.   Swamy, R.N. and M.M. Alasali, *Expansion of Concrete Due to Alkali-Silica Reaction.* Aci Materials Journal, 1988. **85**(1): p. 33-40.
5.   Swamy, R.N. and M.M. Alasali, *Effect of Alkali-Silica Reaction on the Structural Behavior of Reinforced-Concrete Beams.* Aci Structural Journal, 1989. **86**(4): p. 451-459.
6.   Officials, A., *Standard Method Of Test For Accelerated Detection Of Potentially Deleterious Expansion Of Mortar Bars Due To Alkali-Silica Reaction, In Standard Specifications For Transportation Materials And Methods Of Sampling And Testing Part 2b: Tests*. 2006, American Association Of State Highway And Transportation Officials: Washington D.C.
7.   Liu, M., et al., *A nonlinear wave mixing method for detecting Alkali-Silica reactivity of aggregates.* Review of Progress in Quantitative Nondestructive Evaluation, 2012. **1430**(1524-1531).
8.   Multon, S., A. Sellier, and M. Cyr, *Chemo-mechanical modeling for prediction of alkali silica reaction (ASR) expansion.* Cement and Concrete Research, 2009. **39**(6): p. 490-500.
9.   Shen, C.H. and G.S. Springer, *Moisture Absorption and Desorption of Composite-Materials.* Journal of Composite Materials, 1976. **10**(Jan): p. 2-20.
10.   Officials, A.C., *Standard Test Method for Potential Alkali Reactivity of Aggregates (Mortar-Bar Method)*. 2007, ASTM International, West Conshohocken, PA.
11.   Suwito, A., et al., *A mathematical model for the pessimum size effect of ASR in concrete.* Concrete Science and Engineering, 2002. **4**: p. 23-34.
12.   Jin, W., *Alkali-silica reaction in concrete with glass aggregate - A chemo-physico-mechanical approach*. 1998, Columbia University: New York.
13.   Cantrell, J.H., *Substructural organization, dislocation plasticity and harmonic generation in cyclically stressed wavy slip metals.* Proceedings of the Royal Society of London Series a-Mathematical Physical and Engineering Sciences, 2004. **460**(2043): p. 757-780.